Astron. Astrophys. 357, 101–110 (2000)

ASTRONOMY AND ASTROPHYSICS

HS 0822+3542 – a new nearby extremely metal-poor galaxy

A.Y. Kniazev[1], S.A. Pustilnik[1], J. Masegosa[2], I. Márquez[2], A.V. Ugryumov[1], J.-M. Martin[3], Y.I. Izotov[4], D. Engels[5], N. Brosch[6], U. Hopp[7], S. Merlino[2], and V.A. Lipovetsky[1,⋆]

[1] Special Astrophysical Observatory, Nizhnij Arkhyz, Karachai-Circessia, 369167, Russia
[2] Instituto de Astrofisica de Andalucia, CSIC, Aptdo. 3004, 18080 Granada, Spain
[3] Observatoire de Paris-Meudon, 92195 Meudon, France
[4] Main Astronomical Observatory, Goloseevo, Kiev-127, 03680, Ukraine
[5] Hamburger Sternwarte, Gojenbergswerg 112, 21029 Hamburg, Germany
[6] Wise Observatory, Tel-Aviv University, 69978 Tel-Aviv, Israel
[7] Universitätssternwarte München, 81679 München, Germany

Received 11 January 1999 / Accepted 7 March 2000

Abstract. We present the results of spectrophotometry and BVR CCD photometry, as well as integrated HI radio measurements of a new blue compact galaxy (BCG) HS 0822+3542 with extremely low oxygen abundance: 12 + log(O/H) = 7.35, or 1/36 of solar value. The galaxy is the third most metal-deficient BCG after I Zw 18 and SBS 0335–052. Its very high mass fraction of gas (≈ 95% of all visible mass) and blue colours of underlying nebulosity are also similar to those of SBS 0335–052. This suggests that HS 0822+3542 is one of the nearest and dimmest galaxies experiencing a recently-started first star formation (SF) episode. Its properties imply that for such galaxies there is a linear scaling of the main parameters, at least for the baryon mass range (0.3–20)×10^8 $M_\odot$. The total mass estimate indicates that the galaxy is dynamically dominated by a dark matter (DM) halo, which itself is one of the least massive for galaxies.

Key words: galaxies: abundances – galaxies: fundamental parameters – galaxies: individual: HS 0822+3542 – galaxies: starburst – galaxies: photometry

1. Introduction

Since the Searle & Sargent (1972) paper identifying blue compact galaxies (BCGs), that is, low-mass galaxies showing emission line spectra characteristic of HII regions, intense star formation (SF), and oxygen abundances of 1/50–1/3 solar[1], such objects have been considered as young galaxies undergoing one of their first star formation bursts. I Zw 18, a BCG with the lowest known oxygen abundance among the galaxies (O/H ∼ 1/50 $(O/H)_\odot$, Searle & Sargent 1972; Izotov & Thuan 1999), has been suggested as a candidate to be a truly-local young galaxy, experiencing its first short SF episode. The second candidate young galaxy, SBS 0335–052E, with an oxygen abundance of 1/41 $(O/H)_\odot$ (Melnick et al. 1992; Izotov et al. 1997a; Lipovetsky et al. 1999) was discovered 18 years later by Izotov et al. (1990). With only two probable examples, we must be extremely lucky to be witnessing local galaxy formation. The proximity of these probable young galaxies allows one to study their properties in detail and to set important constraints on models of galaxy formation. Such studies are important for understanding the nature of very faint and compact probable primeval galaxies at high redshifts. Most of such galaxies at $z = 3$–5 were discovered only recently (e.g. Steidel et al. 1996; Dey et al. 1998), and it seems that the majority of them are already rather evolved systems. Moreover, the local candidate young galaxies are at least one order of magnitude less massive than the faintest candidate young galaxies at high redshifts, and represent the range of baryon mass (10^8–10^9 $M_\odot$) within which possibly most of primeval galaxies have formed (e.g. Rees 1988).

Evidence for the existence of old low-mass stellar populations was obtained in the last 25 years for most of the studied BCGs (Thuan 1983; Loose & Thuan 1986). Moreover, no conclusive answer has been reached yet about the youth of the few most metal-poor BCG. However, some observational data have been collected lately, which apparently support young ages for these BCGs. Among them we point out:

a) Extremely low abundances of heavy elements in HII regions surrounding young clusters, consistent with theoretical expectations of "metal" yield during a first SF event ($Z < 1/20\ Z_\odot$) (e.g., Pilyugin 1993);

b) Very blue colours outside the location of the current SF burst, consistent with a lack of stars older than 100 Myr (Hunter & Thronson 1995; Papaderos et al. 1998). While the recent analysis of HST data for I Zw 18 by Aloisi et al. (1999) suggests an age of 1 Gyr for the underlying stellar population of the galaxy, Izotov et al. (2000) argue that a self-consistent treatment of all data favours a significantly larger distance to I Zw 18 then adopted by Aloisi et al., and a 100 Myr stellar population;

c) A large amount of neutral gas, making up 99% of all baryonic (luminous) mass (van Zee et al. 1998; Pustilnik et al. 2000);

Send offprint requests to: A. Kniazev (akn@sao.ru)

⋆ Deceased 1996 September 22

[1] 12+log$(O/H)_\odot$ = 8.92 (Anders & Grevesse 1989).

d) Practically zero metallicity for this HI gas, e.g., (O/H) $< 3\times10^{-5}$(O/H)$_\odot$, as reported for SBS 0335–052E (Thuan & Izotov 1997). This emphasizes either an extremely slow evolution on these systems, or a very recent onset of metal production. The latter suggests that the neutral gas clouds in these galaxies are composed of pregalactic material not yet polluted by stellar nucleosynthesis products.

It was suggested recently by Izotov & Thuan (1999), from the analysis of carbon and nitrogen abundances, that several BCGs with O/H $<$ 1/20 (O/H)$_\odot$ in HII regions are good candidate galaxies with a recent first SF episode. Until now, less than ten such galaxies with good abundance determinations are known. Even though the point on the existence of truly young local galaxies is debatable (see, e.g., Kunth & Östlin 1999), the importance of studies of extremely metal-poor galaxies is undoubtful, since they best approximate the properties of primeval galaxies at large redshifts.

In this paper we describe the data obtained for the third most metal-deficient galaxy, HS 0822+3542 with O/H = 1/36 (O/H)$_\odot$. This is one of the *nearest*, and at the same time the *dimmest* candidate young galaxy known.

2. Observations and data reduction

A new extremely metal-poor BCG, HS 0822+3542, was discovered on April 5, 1998, during observations with the 6 m telescope of the Special Astrophysical Observatory (SAO) of the Russian Academy of Sciences (Pustilnik et al. 1999b), in the framework of the Hamburg/SAO survey for emission-line galaxies (Ugryumov et al. 1999). Its J2000 coordinates are: R.A. = $08^{\rm h}25^{\rm m}55\overset{\rm s}{.}0$, Dec. = +35°32′31″. The main parameters of the galaxy are presented in Table 1. Here we present new optical spectroscopic and photometric, and HI 21 cm radio observations to study the properties of this galaxy.

2.1. Long-slit spectroscopy

2.1.1. Observations

Optical spectra of HS 0822+3542 were obtained with the 6 m telescope on April 6, 1998 with the spectrograph SP-124 equipped with a Photometrics CCD-detector (24×24 μm pixel size) and operating at the Nasmyth-1 focus. The grating B0 with 300 grooves/mm provides dispersion of 4.6 Å pixel^{-1} and spectral resolution of about 12 Å at first order. A long slit with a size $2''\times40''$ was used. The scale along the slit was $0\overset{''}{.}4$ pixel^{-1}. The total spectral range covered was $\lambda\lambda$ 3700–8000 Å.

High S/N ratio long-slit spectroscopy was conducted with the 2.5 m Nordic Optical Telescope (NOT) on May 27 and 28, 1998. We used the spectrograph ALFOSC equipped with a Loral (W11-3AC) CCD, with a $1\overset{''}{.}3\times400''$ slit, and grisms #6 and #7 (110 Å/mm), which provide a spectral dispersion of 1.5 Å pixel^{-1} and a resolution of about 8 Å (FWHM). The spectral range was $\lambda\lambda$ 3200–5500 Å for grism #6 and $\lambda\lambda$ 3800–6800 Å for grism #7. The spatial resolution was of $0\overset{''}{.}189$ per pixel. The total exposure time for grism #6 was 60 min, split into three 20 min exposures, and 40 min for grism #7, split into two 20 min exposures. The slit, centred on the brightest knot (see in Fig. 1 the R-band image of the galaxy), was oriented in the N-S direction. Spectra of He-Ne comparison lamp were obtained after each exposure for wavelength calibration, and three spectrophotometric standard stars Feige 34, HZ 44 and BD+33°2642, were observed for flux calibration. The seeing during the spectral observations was $\approx 0\overset{''}{.}8$.

Table 1. Main parameters of the young galaxy candidates

Parameter	0822+3542[1]	IZw18	0335–052E
$B_{\rm tot}$	17.92±0.07	16.21[2]	17.00±0.02[3]
$(B-V)_{\rm tot}$	0.32±0.08	0.18[2]	0.31±0.05[3]
$(V-R)_{\rm tot}$	0.17±0.09	0.41[4]	0.15±0.05[3]
$V_{\rm Hel}$ (km s^{-1})	732±6	751±2[5]	4043±5[6]
$D_{\rm Vir}$(Mpc)	12.5	14.2[1]	52.8[6]
$E(B-V)$	0.047[11]	0.032[11]	0.047[11]
M_B†	–12.7	–14.64	–16.8[3]
Angular size (″)‡	14.8×7.4	22×15[1]	14×10[3]
Optical size (kpc)	0.90×0.45	1.5×1.0	3.7×2.6[3]
12+log(O/H)	7.35	7.16[7]	7.29[8]
$T_{\rm e}$(O III) (K)	20,350	19,600[7]	19,300[8]
H I flux*	0.68±0.07	2.97[9]	2.46[6]
W_{50} (km s^{-1})	42±5	49[9]	83[5]
W_{20} (km s^{-1})	58±8	84[9]	105[5]
M(HI) ($10^8 M_\odot$)	0.24	1.41[9]	16.2[6]
M(HI)/L_B**	1.40	1.40	2.3
SFR ($M_\odot$/year)	0.007	0.04[10]	0.4[10]

$B_{\rm tot}$ – total blue magnitude; M_B – absolute blue mag. L_B – total blue luminosity. * Units of Jy km s^{-1}; ** In units of $(M/L_B)_\odot$; † With the Galaxy extinction A_B = 0.20, 0.14, 0.20, respectively, corresponding to $E(B-V)$ in the previous line; ‡ $a\times b$ at surface brightness μ_B=25 mag arcsec^{-2}.
References: [1]This paper; [2]Mazzarella & Boroson (1993); [3]Papaderos et al. (1998); [4]Huchra (1977); [5]Thuan et al. (1999a); [6]Pustilnik et al. (2000); [7]Izotov & Thuan (1998); [8]Izotov & Thuan (1999); [9]van Zee et al. (1998); [10] Thuan et al. (1997); [11] Schlegel et al. (1998)

2.1.2. Reduction of long-slit spectra

Data reduction was carried out using the MIDAS[2] software package (Grosbøl 1989). Procedures included bias subtraction, cosmic-ray removal and flat-field correction. The flat-field correction was produced with the normalization algorithm described by Shergin et al. (1996). After the wavelength mapping and night sky subtraction, each 2D frame was corrected for atmospheric extinction and was flux calibrated. To derive the sensitivity curves, we used the spectral energy distributions of the standard stars from Bohlin (1996). Average sensitivity curves for grisms were produced for each observing night. R.m.s. deviations between the average and individual sensitivity curves are

[2] MIDAS is an acronym for the European Southern Observatory package — Munich Image Data Analysis System.

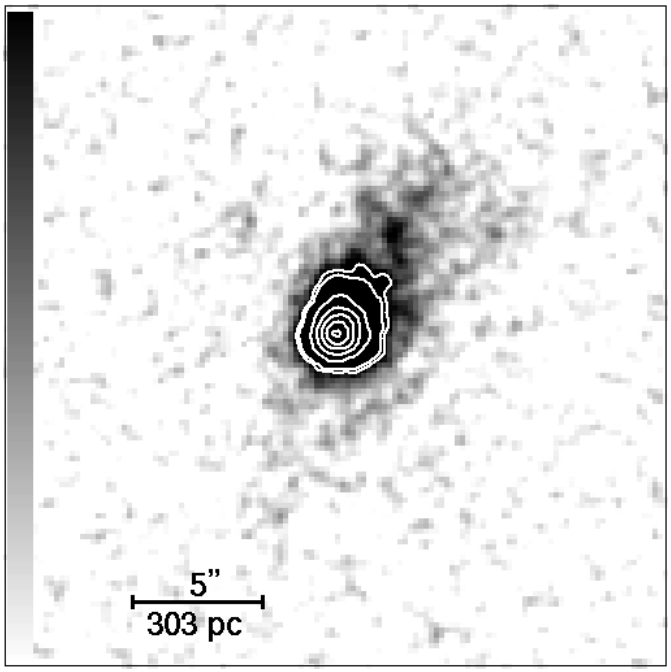

Fig. 1. R-band image of HS 0822+3542. North is to the top, east is to the left. Low-contrast filaments NW of the main bright body indicate gas structures typical of high-velocity ejecta. At the adopted distance of 12.5 Mpc, $1'' = 60.6$ pc. Surface brightness isophotes (white contours) are superposed on the central bright region to show the morphology of supergiant H II region.

Table 2. Line intensities in HS 0822+3542

λ_0(Å) Ion	$F(\lambda)/F(\mathrm{H}\beta)$	$I(\lambda)/I(\mathrm{H}\beta)$
3727 [O II]	0.331 ±0.013	0.331 ±0.014
3835 H9	0.077 ±0.005	0.080 ±0.007
3868 [Ne III]	0.317 ±0.018	0.318 ±0.018
3889 H8 + He I	0.199 ±0.009	0.203 ±0.010
4026 He I	0.026 ±0.005	0.026 ±0.005
4101 Hδ	0.271 ±0.011	0.274 ±0.012
4340 Hγ	0.479 ±0.018	0.481 ±0.018
4363 [O III]	0.123 ±0.007	0.123 ±0.008
4471 He I	0.039 ±0.005	0.039 ±0.005
4861 Hβ	1.000 ±0.033	1.000 ±0.034
4922 He I	0.009 ±0.003	0.009 ±0.003
4959 [O III]	1.192 ±0.042	1.190 ±0.042
5007 [O III]	3.550 ±0.121	3.542 ±0.121
5876 He I	0.098 ±0.005	0.097 ±0.005
6300 [O I]	0.004 ±0.003	0.004 ±0.003
6312 [S III]	0.010 ±0.003	0.010 ±0.003
6548 [N III]	0.005 ±0.004	0.005 ±0.004
6563 Hα	2.743 ±0.087	2.729 ±0.094
6584 [N II]	0.015 ±0.012	0.015 ±0.012
6678 He I	0.033 ±0.004	0.033 ±0.004
6717 [S II]	0.029 ±0.004	0.028 ±0.004
6731 [S II]	0.018 ±0.004	0.018 ±0.004
$C(\mathrm{H}\beta)$ dex	0.005±0.04	
$F(\mathrm{H}\beta)$	0.47×10^{-14} erg s^{-1}cm^{-2}	
$EW(\mathrm{H}\beta)$ Å	292±3	
EW(abs) Å	0.6±0.7	

≈1.5%, with the maximum deviations of ≈4% in the spectral region 3800÷4000 Å.

The 2D flux-calibrated spectra were then corrected for atmospheric dispersion (see Kniazev et al. 2000) and averaged. Finally, the 1D averaged spectrum was extracted from a 0.″8 region along the slit, where $I(\lambda4363\ \text{Å}) > 2\sigma$ (σ is the dispersion of a noise statistics around this line) (see Fig. 2).

Redshift and line fluxes were measured applying Gaussian fitting. For Hα, [NII] $\lambda\lambda$ 6548,6583 Å and [SII] $\lambda\lambda$ 6716,6731 Å a deblending procedure was used, assuming gaussian profiles with the same FWHM as for single lines. The errors of the line intensities in Table 2 take into account the Poisson noise statistics and the noise statistics in the continuum near each line, and include uncertainties of data reduction. These errors have been propagated to calculate element abundances.

The observed emission line intensities $F(\lambda)$, and those corrected for interstellar extinction and underlying stellar absorption $I(\lambda)$ are presented in Table 2. All lines have been normalized to the Hβ intensity. The Hβ equivalent width EW(Hβ), the absorption equivalent widths EW(abs) of the Balmer lines, the Hβ flux, and the extinction coefficient C(Hβ) (this is a sum of internal extinction in HS 0822+3542 and foreground one in the Milky Way) are also shown there.

For the simultaneous derivation of C(Hβ) and EW(abs), and to correct for extinction, we used a procedure described in detail in Izotov et al. (1994). The abundances of the ionized species and the total abundances of O, Ne, N, S, and He have been obtained following Izotov et al. (1994, 1997b) and Izotov & Thuan (1999).

2.2. CCD photometry

2.2.1. Observations

CCD images in Bessel BVR filters were obtained with the NOT and ALFOSC on 1998, May 28. The same 2k×2k Loral (W11-3AC) CCD was used, with a plate scale of 0.″189×0.″189 and a 6.′5×6.′5 field of view. Exposures of 900 s in B and 600 s in both V and R were obtained under photometric conditions but no photometric calibration was performed. The seeing FWHM was 1.″25. Dr. A. Kopylov (SAO RAS) kindly obtained short CCD images in BVR with the 1 m telescope of SAO. These observations were used to calibrate the NOT data. Photometric calibration was provided by observations of the stars #4, #7 and #10 from the field of OJ 287 (Firucci & Tosti 1996; Neizvestny 1995).

2.2.2. Reduction of photometric data

All primary data reduction was done with MIDAS. The frames were corrected for bias, dark, and flat field in the same way as for reduction of the 2D frames of NOT long-slit spectra. Aperture photometry was performed on the standard star frames using the `MAGNITUDE/CIRCLE` task, with the same aperture for

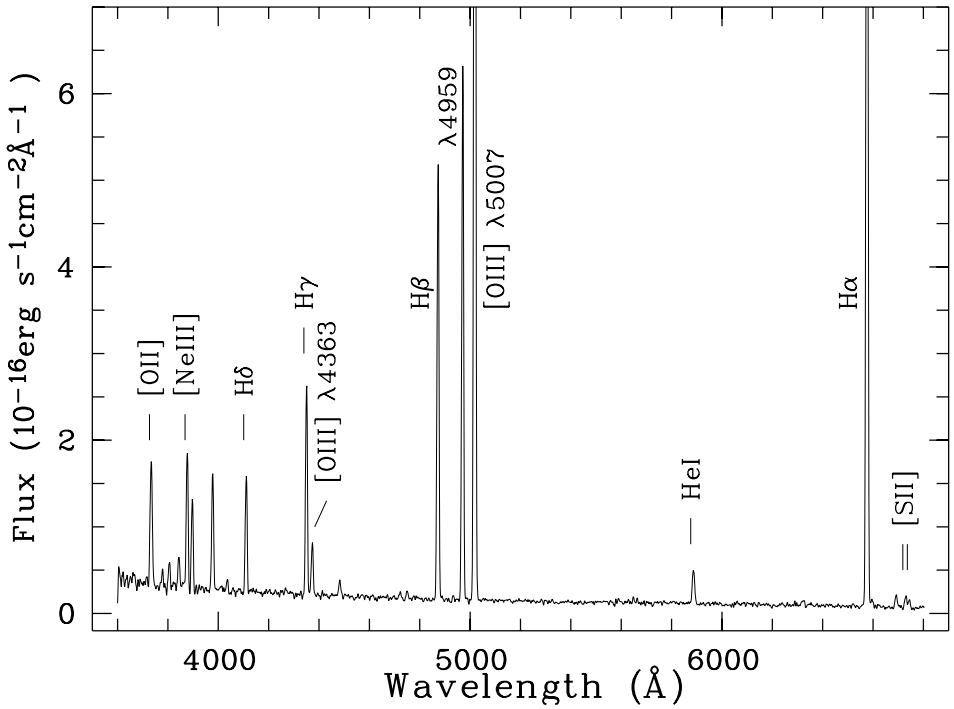

Fig. 2. The observed NOT spectrum of HS 0822+3542 in the aperture $1\farcs3\times0\farcs8$ with nebular emission lines identification.

all stars. The instrumental magnitudes were transformed to the standard photometric system magnitudes via secondary local standards, calibrated with the 1 m telescope of SAO. The final zero-point uncertainties of the transformation were $\sigma_B = 0\overset{\mathrm{m}}{.}06$ in B, $\sigma_V = 0\overset{\mathrm{m}}{.}05$ in V, and $\sigma_R = 0\overset{\mathrm{m}}{.}08$ in R.

For the creation of the sky background, we used the dedicated software for adaptive filtering developed at the Astrophysical Institute of Potsdam (Lorenz et al. 1993).

The photometry of extended objects was carried out with the IRAF[3] software package. Elliptical fitting was performed with the ELLIPSE task in the STSDAS package. To construct a surface brightness (SB) profile we used the equivalent radius as the geometrical average, $R^*=\sqrt{ab}$. The SB profiles were decomposed into two components: one with a gaussian distribution in the central part and the second being an exponential disc. The final function has the form:

$$I = I_{\mathrm{E},0}\exp\left(-\frac{R^*}{\alpha_{\mathrm{E}}}\right) + I_{\mathrm{G},0}\exp\left[-\ln 2\left(2\frac{R^*}{\alpha_{\mathrm{G}}}\right)^2\right] \qquad (1)$$

For the profile decomposition, the NFIT1D task of the STSDAS was used with weights inversely proportional to the accuracy of the surface brightness profile. The final photometric errors take into account the instrumental errors and the error of transformation to the standard photometrical system. To check correctness of disc parameters we performed separately the fitting of external part of SB profile, corresponding to the region in Fig. 5 from R^* of 3″ to 6″. The derived disc parameters were the same within the cited errors.

For consistency with previous works (e.g. Telles et al. 1997, Papaderos et al. 1996, 1998, Doublier et al. 1999a) the parameters of the disc have been obtained by fitting again the SB versus the equivalent radius, but we note that the obtained values should be taken with caution, because of ellipticity variations.

2.3. HI *21 cm observations and data reduction*

HI line observations were carried out in July 1998 and in February 1999 with the Nançay[4] 300m radio telescope (NRT). The NRT has a half-power beam width of $3\farcm7$ (EW) $\times$ $22'$ (NS) at the declination Dec. = 0°.

Since HS 0822+3542 had a known optical redshift, we split the 1024-channel autocorrelator in two halves and used a dual-polarization receiver to increase the S/N ratio. Each correlator segment covered a 6.4 MHz bandwidth, corresponding to a 1350 km s^{-1} velocity coverage, and was centred at the frequency corresponding to the optical redshift. The channel spacing was 2.6 km s^{-1} before smoothing and the effective resolution after averaging pairs of adjacent channels and Hanning smoothing was 10.6 km s^{-1}. The system temperature of the receiver was $\approx$ 40 K in the horizontal and vertical linear polarizations. The gain of the telescope was 1.1 K/Jy at the declination Dec. = 0°. The observations were made in the standard total power (position switching) mode with 1-minute on-source and 1-minute off-source integrations.

[3] IRAF: the Image Reduction and Analysis Facility is distributed by the National Optical Astronomy Observatories, which is operated by the Association of Universities for Research in Astronomy, In. (AURA) under cooperative argeement with the National Science Foundation (NSF).

[4] The Nançay Radioastronomy Station is part of the Paris Observatory and is operated by the Ministère de l'Education Nationale and Institut des Sciences de l'Univers of the Centre National de la Recherche Scientifique.

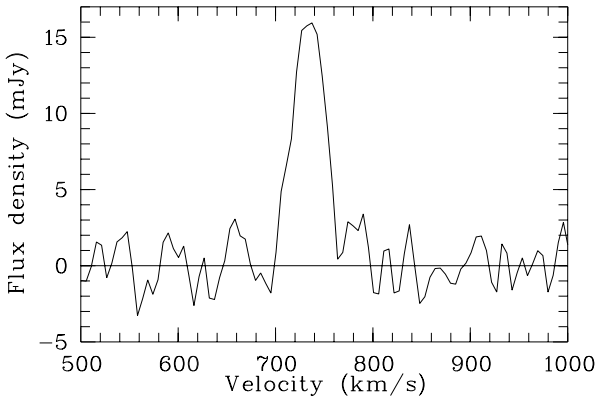

Fig. 3. HI 21 cm profile of HS 0822+3542.

The data were reduced using the NRT standard programs DAC and SIR, written by the telescope's staff. Both H and V polarization spectra were calibrated and processed independently, and were finally averaged together. Error estimates were calculated following Schneider et al. (1986). With an integration time of 210 minutes, the r.m.s. noise is of 1.4 mJy after smoothing. HS 0822+3542 is detected with S/N=11. The spectrum is presented in Fig. 3.

3. Results and discussion

The main parameters of HS 0822+3542, along with those of the two earlier known local candidate young galaxies, are presented in Table 1.

The distances to all three galaxies for the sake of homogeneity are derived from the radial velocities. For the distance-dependent parameters we used the distances $D_{\rm Vir}$ derived from the quoted heliocentric HI velocities $V_{\rm HI}$, accounting for the Galaxy motion relative to the centroid of the Local Group of 220 km s^{-1}, for Virgocentric infall (Kraan-Korteweg 1986), and assuming a Hubble constant H_0 = 75 km s^{-1}Mpc^{-1}. Note that HS 0822+3542 is the *nearest* galaxy among the extremely metal-deficient galaxies shown in Table 1. However, such distance estimates for two galaxies, HS 0822+3542 and I Zw 18 with small radial velocities are rather uncertain. In particular, for I Zw 18 different distance determinations from the literature based on the different observational data, range from 10.9 Mpc to 20 Mpc. To resolve this disagreement the deep HST imaging of I Zw 18 is vital in order to detect the tip of the red giant branch stars and to measure the distance directly. Unfortunately, such observations have not yet been done. The same relates to HS 0822+3542. Keeping in mind this possible source of uncertainty which may change integrated characteristics of HS 0822+3542 and I Zw 18 by a factor of 2–4, we describe below in more detail various parameters of HS 0822+3542 and compare them to other well-known young galaxy candidates.

3.1. Chemical abundances

The results from the chemical abundance determination are presented in Table 3. For the sake of comparison, we also show the data for the other two low metallicity galaxies SBS 0335–052 and I Zw 18. A two-zone photoionized HII region has been assumed; the electron temperature for the high-ionization region has been obtained from the [OIII] λ4363/(λ4959+5007) ratio using a five-level atom model (Izotov & Thuan 1999) and for the low-ionization region by using the empirical relation between both electron temperatures (Izotov et al. 1997b). The electron density was derived from the [SII]λ6717,6731 ratio. Abundances have been calculated following Izotov et al. (1994, 1997b).

The oxygen abundance in HS 0822+3542 is slightly higher than in the other two galaxies. This galaxy is, therefore, one more object filling the gap between the metallicity of I Zw 18 and those for the bulk of BCGs. The comparison of the data on element abundances in HS 0822+3542 with the abundance ratios from Izotov & Thuan (1999) shows that all data for HS 0822+3542 agree with the derived average values for the sample of low-metallicity BCGs. The largest deviation occurs in the N/O ratio. But if we take into account the large uncertainty in the flux of [NII] λ6583 emission line blended with Hα, the N/O is consistent with the expected value for this kind of galaxies.

We thus conclude that the measured ratios of heavy element abundances to that of oxygen in HS 0822+3542 follow the same relation as in all metal-poor BCGs. In particular, nitrogen is likely synthesized in massive stars that also produce oxygen, neon and sulfur, as proposed by Izotov & Thuan (1999).

We note, that low measured value of C(Hβ)=0.005$\pm$0.04, transfered to a 2σ upper limit: C(Hβ) $<$ 0.085, equivalent to $E(B-V)$ = 0.68 C(Hβ) $<$ 0.058, is consistent with $E(B-V)$ = 0.047$\pm$0.007 from Schlegel et al. (1998), which was used to correct measured colours and absolute magnitude. Anyway the net internal extinction A$_B$ in HS 0822+3542 seems to be very low, implying a low dust content, what is also consistent with the object extremely low metallicity.

3.2. Morphology and colours

The R-band image of the galaxy, with filamentary structures at the periphery of the low surface brightness region, is typical of dwarfs with strong SF activity. Curiously, the appearance of HS 0822+3542 is morphologically similar, on the same angular scales, to that of SBS 0335–052E (Melnick et al. 1992; Thuan et al. 1997), including some arcs and filaments. The integrated ($B-V$) and ($V-R$) colours of HS 0822+3542 are very blue ($0\overset{\rm m}{.}32$ and $0\overset{\rm m}{.}17$, respectively), similar to those of SBS 0335–052E.

Below, we describe the surface brightness (SB) distribution of HS 0822+3542. We show in Fig. 4 the SB profiles in B, V and R-bands, which look very similar, with some deviations in R-band in the middle part of the profile. This is presumably due to additional Hα emission from the filamentary structure (see Fig. 1). The B-band SB profile (Fig. 5) indicates the presence of two components: the central bright compact body and an exponential disc, dominating the light in the outer part of the profile (hereafter LSB component). The parameters of both

Table 3. Abundances in HS 0822+3542, SBS 0335–052 and I Zw 18

Value	HS 0822+3542	SBS 0335–052E[1,2]	SBS 0335–052W[3]	I Zw 18NW[4]	I Zw 18SE[4]
T_e(O III)(K)	20,360±850	20,300±300	17,200±500	19,700±200	18,800±400
T_e(O II)(K)	15,790±600	15,800±200	14,700±400	15,600±150	15,300±300
T_e(S III)(K)	18,600±700	18,500±200	16,000±400	18,000±200	17,300±350
N_e(S II)(cm^{-3})	$<10\pm^{40}_{10}$	524±204	10	90	10
$O^+/H^+(\times10^5)$	0.247±0.025	0.20±0.1	0.60±0.05	0.22±0.01	0.49±0.03
$O^{++}/H^+(\times10^5)$	1.967±0.190	1.70±0.1	1.08±0.08	1.16±0.03	1.04±0.06
O/H($\times10^5$)	2.214±0.191	1.90±0.1	1.68±0.10	1.45±0.03	1.54±0.07
12+log(O/H)	7.35±0.04	7.29±0.01	7.22±0.03	7.16±0.01	7.19±0.02
$N^+/H^+(\times10^7)$	0.992±0.770	0.60±0.01	1.72±0.15	0.64±0.02	1.43±0.08
ICF(N)	8.962	8.66	2.81	6.59	3.14
log(N/O)	–1.40±0.34	–1.58±0.03	–1.54±0.06	–1.56±0.02	–1.53±0.04
$Ne^{++}/H^+(\times10^5)$	0.355±0.041	0.27±0.05	0.24±0.03	0.19±0.01	0.23±0.03
ICF(Ne)	1.126	1.13	1.55	1.25	1.48
log(Ne/O)	–0.74±0.07	–0.80±0.03	–0.65±0.06	–0.80±0.01	–0.65±0.04
$S^+/H^+(\times10^7)$	0.424±0.057	0.40±0.1	1.09±0.11	0.35±0.01	0.67±0.03
$S^{++}/H^+(\times10^7)$	2.815±0.873	1.90±0.3	2.15±0.64	1.96±0.21	2.07±0.30
ICF(S)	2.26	2.21	1.29	1.82	1.32
log(S/O)	–1.48±0.09	–1.59±0.04	–1.60±0.08	–1.55±0.03	–1.63±0.04
Y(mean)	0.255±0.013	0.249±0.006	0.238±0.005	0.217±0.005	0.242±0.009

References: [1] Izotov et al. (1997a); [2] Izotov & Thuan (1999); [3] Lipovetsky et al. (1999); [4] Izotov & Thuan (1998).

Table 4. Structural properties of HS 0822+3542 in B,V,R-bands

Band	$\mu_{E,0}$ mag arcsec^{-2} (1)	α_E arcsec (2)	$\mu_{G,0}$ mag arcsec^{-2} (3)	α_G arcsec (4)	P_{25} pc (5)	E_{25} pc (6)	$m_{LSB}\infty$ mag (7)	$m_{SF}\infty$ mag (8)
B	20.96±0.04	1.41±0.02	20.40±0.02	1.58±0.02	118	318	18.22	19.46
V	20.86±0.04	1.42±0.03	19.92±0.02	1.61±0.03	126	333	18.10	18.68
R	20.57±0.08	1.38±0.04	19.79±0.03	1.61±0.03	129	342	17.88	18.60

(1) Central surface brightness of the LSB component obtained from the decomposition of each SB profile, weighted by its photometric uncertainties.
(2) Exponential scale length of the LSB component.
(3) Central surface brightness of the gaussian (SF burst) component.
(4) Effective size (FWHM) of the gaussian (SF burst) component.
(5) Linear extent of the luminous component in excess of the LSB component at a surface brightness level of 25 mag arcsec^{-2}.
(6) Linear extent of the LSB component at a surface brightness level of 25 mag arcsec^{-2}.
(7) Total apparent magnitude of the LSB component estimated by extrapolation of the exponential fitting law to $R^* = \infty$ (Eq. 2).
(8) Total apparent magnitude of the SF component.

components, derived from the fitting of the SB profiles in B, V and R, are given in Table 4.

The corresponding exponential scale lengths are α_E^B = 86±1 pc, α_E^V = 86±2 pc and α_E^R = 84±2 pc. A comparison with the same parameters derived for the LSB component of other BCGs (Papaderos et al. 1996; Papaderos et al. 1998; Doublier et al. 1999a) shows that the scale length of HS 0822+3542 is smaller than that of any BCG studied in the cited works. Even the "ultracompact" dwarf galaxy POX 186 (Doublier et al. 1999b) has a scale length more than twice larger (180 pc). However HS 0822+3542 is not the only extreme case in its small disc "size". At least two galaxies have comparable or smaller scale lengths: GR 8 (Mateo 1998) and Tol 1116–325 (Telles et al. 1997).

Integrating the SB profile of the underlying exponential disc we obtain its total B magnitude:

$$B_{\rm disc} = \mu_{E,0} - 5\log(\alpha_E) - 1.995, \quad (2)$$

where α_E is in arcsec.

With the resulting $B_{\rm disc}$ = 18.$^{\rm m}$22 we can estimate also the luminosity of current SF burst and the corresponding brightening of the galaxy. The brightening is quite modest, about 30%. The light of current burst corresponds to $B_{\rm burst}$ = 19.$^{\rm m}$46 and a luminosity of $M_B = -11.^{\rm m}1$.

Since the scale lengths for the underlying disc in all three bands are identical within small uncertainties (1–1.5%), we can accept as a first approximation that the scale length of the disc is a unique one for B, V and R, equal to the average $<\alpha_E>$ = 1.40±0.02 arcsec, and corresponding to 85±1 pc. Hence, the

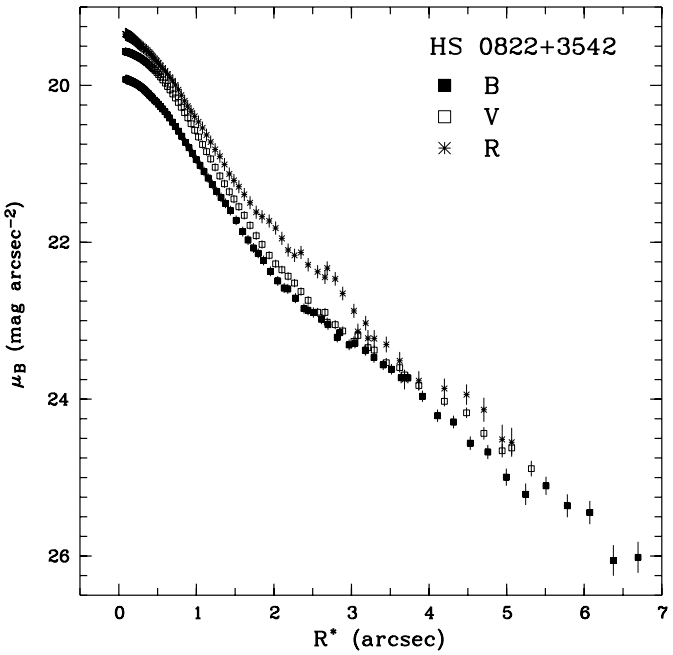

Fig. 4. The surface brightness profiles of HS 0822+3542 in B, V and R-bands. Error bars correspond to 2σ uncertainties.

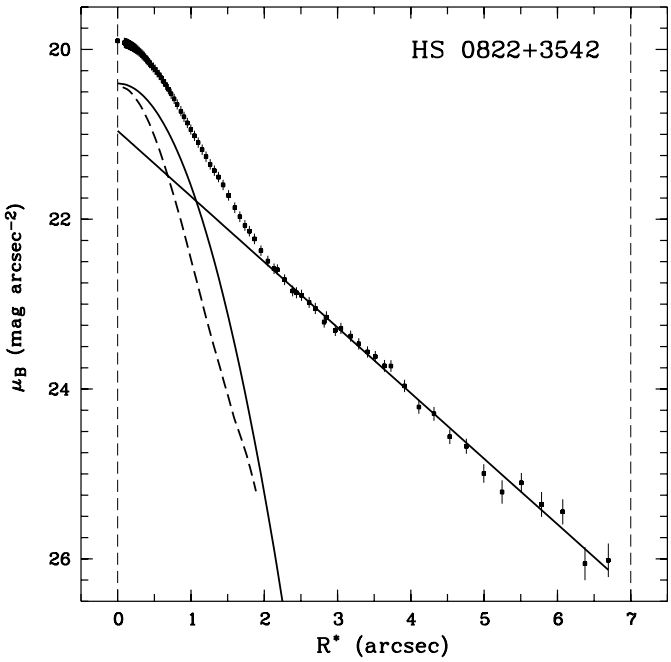

Fig. 5. The surface brightness profile of HS 0822+3542 in B-band. Error bars correspond to 2σ uncertainties. By the solid lines the decomposition of SB profile is shown to the underlying exponential disc and the central gaussian component corresponding to the SF burst region. The decomposition was performed with the weights. Thick dashed line shows the PSF derived on nearby stars, with FWHM = 1.″25. Two vertical dashed lines mark the region over which the decomposition was performed.

underlying disc has no colour gradient, and its colours $(B-V)_{\rm disc}$ and $(V-R)_{\rm disc}$ can be approximated by the colours of its central SB

$$(B-V)_{\rm disc} = \mu^B_{\rm E,0} - \mu^V_{\rm E,0} = 0\overset{\rm m}{.}10 \pm 0\overset{\rm m}{.}06,$$

$$(V-R)_{\rm disc} = \mu^V_{\rm E,0} - \mu^R_{\rm E,0} = 0\overset{\rm m}{.}29 \pm 0\overset{\rm m}{.}09,$$

respectively. The disc colours can also be obtained from its integral B, V and R magnitudes (Column 7 in Table 4):

$$(B-V)_{\rm disc} = 0\overset{\rm m}{.}12 \pm 0\overset{\rm m}{.}10,$$

$$(V-R)_{\rm disc} = 0\overset{\rm m}{.}22 \pm 0\overset{\rm m}{.}16,$$

consistent with the estimates above. The uncertainties of the latter colours are derived from the errors of the integrated disc magnitudes, from the propagation of errors in Eq. (2). They are $0\overset{\rm m}{.}07$, $0\overset{\rm m}{.}08$ and $0\overset{\rm m}{.}14$ for B, V and R, respectively.

A close coincidence of the scale lengths of BCG LSB components in the different filters was found by Papaderos et al. (1998) for SBS 0335–052E. The same correlation for disc scale lengths in different bands was shown to exist for a sample of 19 BCGs (Doublier et al. 1999a). However, the colours $(B-R)_{\rm disc}$ for BCGs with small scale lengths from Doublier et al. are redder and lie in the range of $0\overset{\rm m}{.}61$–$1\overset{\rm m}{.}47$, with an average $(B-R)_{\rm disc} = 1\overset{\rm m}{.}11 \pm 0\overset{\rm m}{.}30$. The most similar to HS 0822+3542 in this colour (with $(B-R)_{\rm disc} = 0\overset{\rm m}{.}61$) is SBS 0940+544, with 12+log(O/H) = 7.43±0.01 (Izotov & Thuan 1999).

In Fig. 6 we show the distributions of observed $(B-V)$ (filled squares) and $(V-R)$ (open circles) colours, as functions of the effective radius. Mean disc colours are shown by filled and open rectangles to the right of the observed colour profiles.

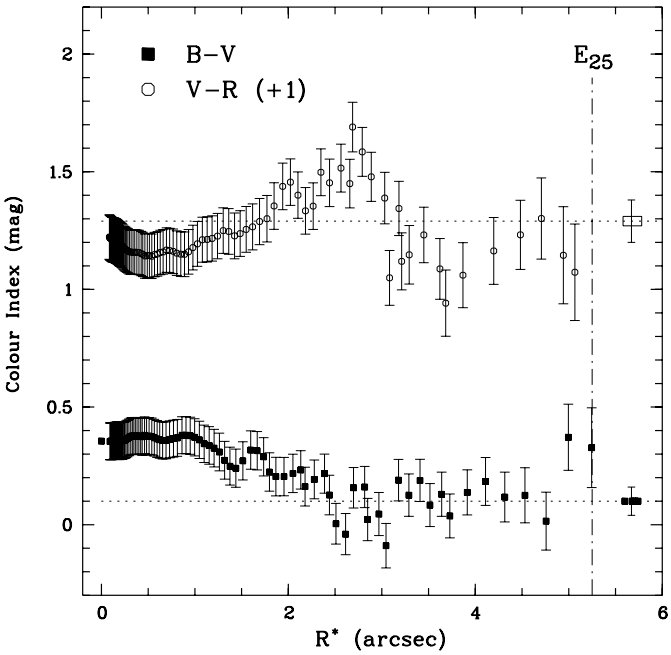

Fig. 6. $(B-V)$ and $(V-R)$ radial colour profiles of HS 0822+3542. Radially averaged $(B-V)$ and $(V-R)$ colour profiles computed by subtraction of surface brightness profiles displayed in Fig. 4. The mean colours of the exponential disc are shown by the filled and open rectangulars with error bars. The isophotal radius E_{25} of the LSB host at 25 B mag arcsec^{-2} is indicated.

Note that the $(V-R)$ colours are shifted by $1\overset{\mathrm{m}}{.}0$ in Fig. 6, to minimize confusion. Note also that $(V-R)$ is even bluer for the outermost part of disc ($R^* > 3''$): $0\overset{\mathrm{m}}{.}16 \pm 0\overset{\mathrm{m}}{.}12$.

Effective sizes for the central gaussian component in the different bands also coincide, within small uncertainties. We can therefore think of this component as a body with a homogeneous colour distribution. We note also, that this compact gaussian component is significantly larger than we could expect for a point-like source convolved with the point spread function (PSF). The FWHM for stellar images measured on the CCD frames near the galaxy is $1\overset{''}{.}25$, whereas it is $\alpha_{\mathrm{G}}=1\overset{''}{.}6$ (Table 4) for the bright central region. The deconvolved FWHM for this component amounts to $\approx 1\overset{''}{.}0$. Comparing with the structure of star-forming regions in other BCGs, it is natural to assign the enhanced optical emission in the central part of HS 0822+3542 to a young massive-star cluster formed in the current SF burst and its associated HII region. The characteristic linear radius of this complex is ~ 30 pc, comparable to the size of the star cluster R136 in LMC (Walborn 1991). Accordingly, the absolute B magnitude of this bright component $-11\overset{\mathrm{m}}{.}1$ is near the lower limit of the range found with HST for super-star clusters by O'Connel et al. (1994) in two nearby star-bursting galaxies.

The total size of HS 0822+3542 out to the μ_B=25 mag arcsec^{-2} isophote can be approximated by an ellipse with major and minor axes $14\overset{''}{.}8$ and $7\overset{''}{.}4$, or 900 by 450 pc, respectively.

As we have shown above, the SB distribution of HS 0822+3542 can be fitted by two components. While the brighter and more compact central component seemingly corresponds to the complex of young massive stars formed during the current SF burst and its associated HII region, the underlying exponential disc can consist of older stars. The latter could be formed either during a previous much earlier SF episode, or relatively recently, in a precursor of the current SF burst, which could be significantly displaced ($\sim$150–200 pc) from the underlying disc centre. If the current SF burst and the previous SF activity are causally connected, the propagation time of the SF wave from the underlying disc centre, with a typical velocity of 10 km s^{-1} (e.g., Zenina et al. 1997) would be only 15–20 Myr. In order to check this option one could search for the HeI absorption features of early B stars in the underlying disc.

To check for emission from older stellar populations, which may reside in the region outside the current SF burst, we compare the colours of underlying disc with those predicted for various models, as well as with similar parameters for other young galaxy candidates.

The very blue colours of the disk, after correcting for the extinction in the Galaxy $(B-V)_0 = 0\overset{\mathrm{m}}{.}05 \pm 0\overset{\mathrm{m}}{.}06$ and $(V-R)_0 = 0\overset{\mathrm{m}}{.}26 \pm 0\overset{\mathrm{m}}{.}09$ are reasonably consistent with the predictions for an instantaneous SF burst with a Salpeter IMF, a metallicity of 1/20 $Z_\odot$ and an age of $\sim$ 100 Myr (Leitherer et al. 1999). If prolonged star formation is assumed, then the age of the oldest stellar population in the extended disc can be larger than that of the instantaneous burst. The observed colours can also be explained by continuous SF with a constant star formation rate from 500 Myr to 20 Myr ago. However, older stellar populations with an age of 10 Gyr are excluded. The derived age is somewhat lower for the outermost part of the of the disc with a bluer $(V-R)$ colour in comparison to its average value. Integrated colours of ionized gas are about $(B-R) = 0\overset{\mathrm{m}}{.}6$–$0\overset{\mathrm{m}}{.}8$ (Izotov et al. 1997a), what is redder than our observed values in the underlying disc. Therefore if some gas emission inputs to the integrated disc colours, then the true colours of stellar component should be even bluer than measured.

These colours are very similar to those of the underlying nebulosity in SBS 0335–052. The latter colours are shown to be well explained by the radiation of ionized gas and A-stars with the ages of no more than 100 Myr, created in the current SF episode. This SF episode is prolonged and may represent a propagating SF wave (Papaderos et al. 1998), similar to what is suggested for another candidate young galaxies I Zw 18 (Izotov et al. 2000) and CG 389 (Thuan et al. 1999b). This similarity of LSB disc colours of HS 0822+3542 and SBS 0335–052E suggests that up to the radial distances of $\sim$300 pc the input of stellar population with the ages larger than 100 Myr to the disc radiation is undetectable.

As a first approximation, the colours of the underlying disc do not contradict the possibility that the current burst is the first SF episode in this galaxy. However since the emission of ionized gas can add significantly to the total radiation from the volume within 300–400 pc, further photometric and spectroscopic observations of HS 0822+3542 are required to account properly for the contribution of gaseous emission.

3.3. Current star formation rate

The star formation rate (SFR) of the current SF episode can be estimated from the total Hα luminosity. The Hα flux was measured within the slit, and was corrected for the missing light outside the slit. A correction factor of 2.33 was calculated, using the brightness profile along the slit and assuming circular symmetry. For the derived total flux F(Hα)=5.8×10^{-14} erg s^{-1} cm^{-2} we obtain a total Hα luminosity of 10^{39} erg s^{-1}.

This Hα luminosity corresponds to a current SFR of ~ 0.007 $M_\odot$ yr^{-1} (Hunter & Gallagher 1986) assuming a Salpeter IMF with a 0.1 $M_\odot$ lower mass cutoff. The gaseous mass converted into the stars during a 3 Myr burst is $\sim 2\times10^4$ $M_\odot$. The unknown contribution of the gaseous emission to the light from the LSB component further complicates the stellar mass estimate. If only stars with age $\leq$ 100 Myr contribute to the LSB luminosity, then the total mass of stars in the underlying disc with $M_{B,\mathrm{disc}}$=$-12\overset{\mathrm{m}}{.}3$ is 1.3×10^6 $M_\odot$ (from e.g., Leitherer et al. 1999). This is much smaller than the total neutral gas mass of $\approx 3.0\times10^7$ $M_\odot$, accounting for a helium mass fraction of 0.25.

The total mass of ionized gas can be obtained from the average mass density inside the HII region and its volume. An average mass density corresponding to the average electron density N_{e} of 1 cm^{-3} within a volume with a diameter of 0.5 kpc yields a total ionized gas mass of 10^6 $M_\odot$.

The above estimates show that baryonic matter in HS 0822+3542 is dominated by the gaseous component.

3.4. HI *and dynamical mass*

The integrated HI line flux, the characteristic widths of 21 cm line profile W_{50} and W_{20} (for a Hanning smoothing of 10.6 km s^{-1}), and the derived HI mass $M_{\rm HI}$ for HS 0822+3542 are presented in Table 1. The small HI mass $2.4\times10^7 M_\odot$ of this galaxy is consistent with its low optical luminosity. The very narrow HI profile is indicative of its very low amplitude of rotational velocity, which does not exceed 30 km s^{-1}. It is difficult to assess the inclination angle correction, since the optical morphology can be unrelated to global properties of the associated HI cloud, as exemplified by the case of SBS 0335–052 (Pustilnik et al. 2000). The role of chaotic gas motions is, in general, more important in very low mass galaxies, where the amplitude of random velocities reaching ten km s^{-1} or more can be commensurate with the rotational velocity.

The measured HI mass and the profile width are in the range characteristic of very low mass galaxies. The mass-to-light parameter M(HI)/L_B = 1.40 $M_\odot/L_\odot$, is comparable to those of I Zw 18 and SBS 0335–052E. It is not as high as in some gas-rich dwarfs from van Zee et al. (1997), but these galaxies, although they have a few HII regions, are in relatively quiescent state. The extremely metal-poor BCGs discussed here experience significant luminosity enhancement due to very intense current and recent SF activity; this results in a significant decrease of their mass-to-light ratios relative to their non-active state.

A rough estimation can be made also on the dynamical mass of HS 0822+3542. From the width of HI profile at the 20% level, a maximum rotation velocity of 30 km s^{-1} can be assumed. The extent of the HI cloud associated with a BCG is normally many times larger than its optical size. The optical radius R_{25} is the radius of a disc galaxy at the isophotal level μ_B = 25.0 mag arcsec^{-2}. A conservative lower limit to the ratio of HI-to-optical radii is 4 (see, e.g. Taylor et al. 1995; Chengalur et al. 1995; Salzer et al. 1991; van Zee et al. 1998; Pustilnik et al. 2000). By equating gravitation and centrifugal force at the edge of HI disc an estimate of the dynamical mass inside 1.5 kpc is obtained; this is 3.4×10^8 $M_\odot$, one order of magnitude larger than the total visible mass of the galaxy $M_{\rm neutral}$ + $M_{\rm stars}$ + $M_{\rm HII\ region}$.

Even rather unprobable case of HI radius equal to the optical one results in the total dynamical mass ∼3 times higher than the visible mass. Hence, HS 0822+3542 like other extremely metal-deficient dwarf galaxies, is dynamically dominated by a dark matter halo, supporting the modern view of primeval galaxy formation process (e.g. Rees 1988). In turn the mass of its DM halo is one of the smallest for galaxies.

4. A candidate young galaxy?

The properties of HS 0822+3542 presented above (extremely low abundance of heavy elements, very blue colour of underlying nebulosity, and extremely small mass ratio of stars to neutral gas) suggest that this could be the nearest candidate young dwarf galaxy forming its first stellar generation. However, on the basis of the present data, we cannot exclude the presence of an underlying older stellar populations originating from earlier SF episodes.

Similar studies of the two previously known young galaxy candidates I Zw 18 and the pair SBS 0335–052E/0335–052W (Izotov et al. 1997a; Thuan & Izotov 1997; Pustilnik et al. 1997; Lipovetsky et al. 1999) have not been conclusive whether such young systems really do exist.

While the chemical properties (see Table 3) of these candidates seem to follow a general trend and behave quite homogeneously, other global properties have still to be understood. From Table 1 it appears that they cover a broad range of neutral hydrogen masses and blue luminosities (a factor of $\sim$ 40–60). The same is true for their current SFRs and for the mass of stars formed in a single star formation episode.

We suggest that a simple linear scaling between several important parameters holds for forming galaxies, at least in the range of baryon masses of (0.3–20)$\times10^8$ $M_\odot$ (see Table 1, and assuming that most of baryons in these BCGs are in atomic hydrogen and helium). This is important both for the analysis of conditions capable of maintaining pristine gas clouds stable for $\sim$ a Hubble time, and for the planning of further searches for such objects. In particular, such low-mass objects can represent a significant fraction of the Lyα absorbers at high redshifts.

One more indirect argument for the possible youth of the three BCGs considered here comes from the calculations of mass and heavy elements loss in dwarfs with active SF (Mac Low & Ferrara 1999). These show that the rate of metal loss is strongly dependent on the baryon mass in the range of 10^7 to 10^9 $M_\odot$. Therefore, if these extremely metal-poor galaxies with masses ranging from 3×10^7 to 2.5×10^9 $M_\odot$ were not in their first SF episode, we should expect significant differences in their observational properties. For the three BCGs discussed here we do not find these differences.

From the surface density of already known objects with extremely low metallicity and small radial velocity one can expect to find at least ten more such galaxies within 15 Mpc, if the search will be extended to the entire sky.

5. Conclusions

From the data and discussion above we reach the following conclusions:

1. HS 0822+3542 is a new nearby (D = 12.5 Mpc) galaxy with oxygen abundance 12 + log(O/H) = 7.35. After I Zw 18 and SBS 0335–052 this is the third lowest metallicity object among Blue Compact Galaxies.
2. Its very low metallicity, very small stellar mass fraction (0.05 relative to the entire baryon mass) and blue colours of the underlying disc [$(B-V)_0 = 0\overset{\rm m}{.}05$, $(V-R)_0 = 0\overset{\rm m}{.}26$] imply that this is one of the few candidates to be a local young galaxy, forming its first generation of stars.
3. HS 0822+3542 is 50–60 times less luminous and massive than another candidate young galaxy SBS 0335–052. This implies a broad range of global parameters for the candidate young galaxies. A linear scaling between several important

parameters of such galaxies probably exists, including parameters related to the SF burst.

4. The dynamical mass estimate using the width of the HI profile and a typical HI gas extent relative to the optical size, leads to the conclusion that HS 0822+3542 is dynamically dominated by a dark matter halo.
5. Higher S/N long-slit spectra than presented here, and deep Hα images are needed to follow the ionized gas extent. Resolved HI maps will be very helpful to study the dynamics of its ISM and the parameters of its DM halo.

Acknowledgements. The authors thank A.I.Kopylov for BVR calibration frames. This work was partly supported by the INTAS grant 96-0500. The SAO authors acknowledge partial support from the Russian Foundation for Basic Researches by grant No. 97-2-16755 and the Center for Cosmoparticle Physics "Cosmion". Part of the data presented here have been taken using ALFOSC, which is owned by the Instituto de Astrofisica de Andalucia (IAA) and operated at the Nordic Optical Telescope under agreement between IAA and the NBIfA of the Astronomical Observatory of Copenhagen. One of us (AK) acknowledges the support by the Junta de Andalucia during his stay at the IAA. The authors thank the anonymous referee for useful suggestions which allowed to improve the presentation of several points. The authors acknowledge the use of the NASA/IPAC Extragalactic Database (NED) and Lyon-Meudon Extragalactic Database (LEDA).

References

Aloisi A., Tosi M., Greggio L., 1999, ApJ 118, 302
Anders E., Grevesse N., 1989, Geochim. Cosmochim. Acta 53, 197
Burstein D., Heiles C., 1982, AJ 87, 1165
Dey A., Spinrad H., Stern D., Graham J.R., Chaffee F.H., 1998, ApJ 498, L93
Bohlin R.C., 1996, AJ 111, 1743
Chengalur J.N., Giovanelli R., Haynes M.P., 1995, AJ 109, 2415
Doublier V., Caulet A., Comte G., 1999a, A&A, in press
Doublier V., Kunth D., Courbin F., Magain P., 1999b, A&A, in press
Firucci M., Tosti G., 1996, A&AS 116, 403
Grosbøl P., 1989, In: Clark G. (ed.) Reviews in modern astronomy 2, p. 242
Huchra J.P., 1977, ApJS 35, 171
Hunter D.A., Gallagher J.S., 1986, PASP 98, 5
Hunter D.A., Thronson H.A., 1995, ApJ 452, 238
Izotov Y.I., Lipovetsky V.A., Chaffee F.H., et al., 1997a, ApJ 476, 698
Izotov Y.I., Lipovetsky V.A., Guseva N.G., Kniazev A.Y., Stepanian J.A., 1990, Nat 343, 238
Izotov Y.I., Papaderos P., Thuan T.X., et al., 2000, A&A, in press
Izotov Y.I., Thuan T.X., 1998, ApJ 497, 227
Izotov Y.I., Thuan T.X., 1999, ApJ 511, 639
Izotov Y.I., Thuan T.X., Lipovetsky V.A., 1994, ApJ 435, 647
Izotov Y.I., Thuan T.X., Lipovetsky V.A., 1997b, ApJS 108, 1
Kniazev A.Y., Pustilnik S.A., Ugryumov A.V., Kniazeva T.F., 2000, Astronomy Letters 26, 163
Kraan-Korteweg R.C., 1986, A&AS 66, 255
Kunth D., Östlin G., 1999, A&AR, in press (astro-ph/9911094)
Leitherer C., Schaerer D., Goldader J.D., et al., 1999, ApJS 123, 3
Lipovetsky V.A., Chaffee F.H., Izotov Y.I., et al., 1999, ApJ 519, 177
Loose H.-H., Thuan T.X., 1986, In: Kunth D., Thuan T.X., Van J.T.T. (ed.) Star Forming Dwarf Galaxies and Related Objects. Editions Frontieres, p. 73
Lorenz H., Richter G., Capaccioli M., Longo G., 1993, A&A 277, 321
Mac Low M.-M., Ferrara A., 1999, ApJ 513, 142
Mateo M., 1998, ARA&A 36, 435
Mazzarella J.M., Boroson T.A., 1993, ApJS 85, 27
Melnick J., Heidary-Malayeri M., Leisy P., 1992, A&A 253, 16
Neizvestny S.I., 1995, In: IAU Colloquium Photometric Systems and Standard Stars. Moletai Astronomical Observatory, Lithuania, August 14–18, p. 37
O'Connel R.W., Gallagher J.S., Hunter D.A., 1994, ApJ 433, 65
Papaderos P., Izotov Y.I., Fricke K.J., Guseva N.G., Thuan T.X., 1998, A&A 338, 43
Papaderos P., Loose H.-H., Thuan T.X., Fricke K.J., 1996, A&AS 120, 207
Pilyugin L.S., 1993, A&A 277, 42
Pustilnik S.A., Brinks E., Thuan T.X., Lipovetsky V.A., Izotov Y.I., 2000, AJ, submitted
Pustilnik S.A., Engels D., Ugryumov A.V., et al., 1999b, A&AS 137, 299
Pustilnik S.A., Lipovetsky V.A., Izotov Y.I., et al., 1997, Astronomy Letters 23, 308
Rees M., 1988, Highlights of Astronomy 8, 45
Salzer J.J., di Serego Alighieri S., Matteucci F., Giovanelli R., Haynes M.P., 1991, AJ 101, 1258
Schlegel D.J., Finkbeiner D.P., Douglas M., 1998, ApJ 500, 525
Schneider S.E., Helou G., Salpeter E.E., Terzian Y., 1986, AJ 92, 742
Searle L., Sargent W.L.W., 1972, ApJ 173, 25
Shergin V., Kniazev A., Lipovetsky V.A., 1996, Astronomische Nachr. 317, 95
Steidel C., Giavalisco M., Pettini M., Dickinson M., Adelberger K., 1996, ApJ 462, L17
Taylor C.L., Brinks E., Grashius R.M., Skillman E.D., 1995, ApJS 99, 427
Telles E., Melnick J., Terlevich R., 1997, MNRAS 288, 78
Thuan T.X., 1983, ApJ 268, 667
Thuan T.X., Izotov Y.I., 1997, ApJ 489, 623
Thuan T.X., Izotov Y.I., Foltz C.B., 1999b, ApJ 525, 105
Thuan T.X., Izotov Y.I., Lipovetsky V.A., 1997, ApJ 477, 661
Thuan T.X., Lipovetsky V.A., Martin J.-M., Pustilnik S.A., 1999a, A&AS 139, 1
Ugryumov A.V., Engels D., Lipovetsky V.A., et al., 1999, A&AS 135, 511
van Zee L., Haynes M.P., Salzer J.J., 1997, AJ 114, 2497
van Zee L., Westpfahl D., Haynes M., Salzer J.J., 1998, AJ 115, 1000
Walborn N.R., 1991, In: Leitherer C., Walborn N.R., Heckman T.M., Norman C.A. (eds.) Massive Stars in Starbursts. Cambridge Univ. Press, Cambridge, p. 145
Zenina O.A., Balinskaya I.S., Kniazev A.Y., Lipovetsky V.A., 1997, Astronomy Reports 41, No.4, 472